

Stable excitations and holographic transportation in tensor networks of critical spin chains

Zuo Wang^{1,2,3} and Liang He^{1,2,3,*}

¹*Institute for Theoretical Physics, School of Physics,*

South China Normal University, Guangzhou 510006, China

²*Key Laboratory of Atomic and Subatomic Structure and Quantum Control (Ministry of Education), Guangdong Basic Research Center of Excellence for Structure and Fundamental Interactions of Matter,*

School of Physics, South China Normal University, Guangzhou 510006, China

³*Guangdong Provincial Key Laboratory of Quantum Engineering and Quantum Materials,*

Guangdong-Hong Kong Joint Laboratory of Quantum Matter,

South China Normal University, Guangzhou 510006, China

The AdS/CFT correspondence conjectures a duality between quantum gravity theories in anti-de Sitter (AdS) spacetime and conformal field theories (CFTs) on the boundary. One intriguing aspect of this correspondence is that it offers a pathway to explore quantum gravity through tabletop experiments. Recently, a multi-scale entanglement renormalization ansatz (MERA) model of AdS/CFT that can be implemented using contemporary quantum simulators has been proposed [R. Sahay, M. D. Lukin, and J. Cotler, arXiv:2401.13595 (2024)]. Particularly, local bulk excitations (entitled “hologrons”) manifesting attractive interactions given by AdS gravity were found. However, the fundamental question concerning the stability of these identified hologrons is still left open. Here, we address this question and find that hologrons are unstable during dynamic evolution. In searching for stable bulk excitations with attractive interactions, we find they can be constructed by the local primary operators in the boundary CFT. Furthermore, we identify a class of boundary excitations that exhibit the bizarre behavior of “holographic transportation”, which can be directly observed on the boundary system implemented in experiments.

Introduction.—The AdS/CFT correspondence is a cornerstone in the exploration of quantum gravity [1–3]. It conjectures that the quantum gravity theory in a $(d+1)$ -dimensional anti-de Sitter (AdS) spacetime is equivalent to a conformal field theory (CFT) without gravity on the d -dimensional boundary. This duality provides a concrete realization of the holographic principle in quantum gravity [4, 5], with a prominent example being the duality between type IIB superstring theory on $\text{AdS}_5 \times \text{S}^5$ and $\mathcal{N} = 4$ super Yang-Mills theory in four dimensions [1]. The correspondence has also been extended to other dimensions, with the $\text{AdS}_3/\text{CFT}_2$ case being particularly notable due to the tractability of 2D CFTs, such as the 2D Ising CFT [6], which facilitates non-perturbative investigations of quantum gravity and black hole physics in AdS_3 through quantum simulations of the boundary theory. These boundary theories, as low-energy effective descriptions of critical quantum systems, are increasingly accessible to experimental realization, thanks to recent advances in quantum simulation platforms—such as trapped ions [7, 8], Rydberg atom arrays [9–11], and ultracold atoms in optical lattices [12]—which are opening new avenues for exploring gravitational physics in a controlled laboratory setting.

To bridge the gap between theoretical advancements and experimental realizations, various models have been proposed, such as the SYK model [13–17] and the BFSS matrix model [18–24]. While these models have attracted significant interest, their large-scale simulations remain technically challenging [24–26]. In contrast, tensor network approaches, particularly the multi-scale entangle-

ment renormalization ansatz (MERA), offer a promising framework for exploring holographic mappings [27–29]. MERA provides an exact unitary mapping between a boundary CFT and a bulk system [30, 31], capturing the AdS/CFT correspondence at the level of Hilbert spaces [32] and potentially yielding holographic dictionaries such as the GKPW relation [2, 3] and the BDHM relation [33]. Recently, Ref. [34] introduced a MERA-based model mapping a $(1+1)$ -dimensional critical spin chain to a $(2+1)$ -dimensional bulk spin system, unveiling “hologrons”, massive bulk excitations that experience an attractive force akin to gravity in AdS spacetime. This work establishes a compelling gravitational analogy, sparking interest in whether such models can capture gravitational dynamics, such as particle interactions and black hole dynamics. However, the stability of these hologrons remains an open question, representing a crucial step toward validating the model’s capacity to probe gravitational dynamics. If hologrons prove unstable, identifying a stable quasiparticle becomes crucial. Moreover, it remains uncertain whether the model captures a broader range of gravitational phenomena and AdS/CFT physics beyond the observed attractive forces.

In this work, we address the open questions related to the experimentally accessible holographic model for AdS/CFT proposed in Ref. [34], where a critical spin chain is unitarily mapped to a bulk MERA tensor network, and obtain the following key results. (i) We show that hologrons are dynamically unstable. (ii) We identify a class of dynamically stable bulk quasiparticles, constructed from the local primary operators of the bound-

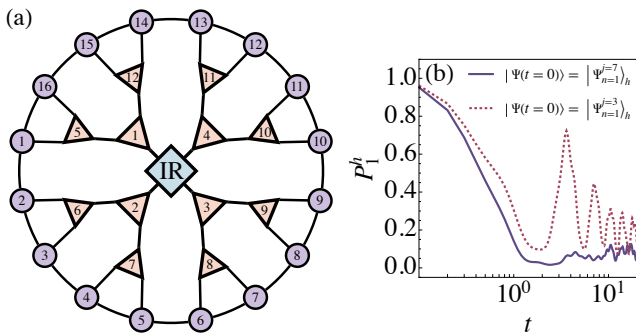


Figure 1. Hologron stability in the MERA model. (a) Physical degrees of freedom in the MERA tensor network [34] implemented in the simulation. The circles represent the spins on the boundary critical spin chain, the triangles correspond to bulk spins, and the square at the center indicates the infrared degree of freedom of the bulk system. (b) Time evolution of $P_1^h(t)$ with initial bulk states $|\Psi_{n=1}^{j=7}\rangle_h$ and $|\Psi_{n=1}^{j=4}\rangle_h$. See text for more details.

ary CFT. These quasiparticles are localized, massive, and exhibit attractive interactions, therefore they could be good candidates for exploring gravitational physics in holographic models. (iii) We observe a bizarre phenomenon, termed “holographic transportation”, rooted in the AdS/CFT correspondence, in which boundary excitations temporarily vanish from the boundary and undergo a process analogous to being “transported” along AdS geodesics via the extra dimension of the holographic AdS bulk. Moreover, we find that this holographic transportation, a phenomenon deeply rooted in the AdS/CFT correspondence, is robust against typical experimental imperfections, making it a highly promising candidate for direct observation in state-of-the-art quantum simulation platforms, such as programmable Rydberg atom arrays [9, 34–39].

Hologrons and their instability.—We consider the holographic model proposed in Ref. [34] that is accessible to experimental simulations on current quantum simulation platforms. It consists of a unitary mapping between a $(1+1)$ -dimensional critical spin chain on the boundary and a $(2+1)$ -dimensional “bulk” system [see Fig. 1(a) for a schematic illustration]. More specifically, the critical spin chain on the boundary is described by the Hamiltonian H_∂ , which takes the explicit form:

$$H_\partial = J \frac{L}{4\pi} \sum_{j=1}^L (X_{j-1} Z_j X_{j+1} - X_j X_{j+1}), \quad (1)$$

where X, Y, Z are Pauli operators, J is the interaction energy, L is the total number of lattice sites, and periodic boundary conditions are assumed. Throughout this study, we work in units where $J = 1$ and $\hbar = 1$. The bulk system consists of $L - 4$ bulk spins [triangle in Fig. 1(a)] and a core region [square in Fig. 1(a)]. Its Hamiltonian H is related to the boundary system H_∂ via the holographic

unitary map \mathcal{U} , i.e., $H = \mathcal{U}^\dagger H_\partial \mathcal{U}$, where \mathcal{U} is derived from the MERA [28, 29, 40] tensor network representation of the ground state of the critical spin chain H_∂ . We use the class of scale-invariant MERA [41], which allows for an analytical expression of \mathcal{U} (see Supplemental Material (SM) [42] for technical details).

The ground state of the bulk system $|\Psi_{\text{GS}}\rangle$ takes the form $|\Psi_{\text{GS}}\rangle = |0\rangle^{\otimes(L-4)} \otimes |\psi_0\rangle$ within MERA. Here, $|0\rangle$ ($|1\rangle$) is the eigenstate of Pauli operator Z for each bulk spin with the higher (lower) eigenvalue, and the states $\{|\psi_k\rangle\}$ for $k = 0, \dots, 15$ form a basis for the core region, with a Hilbert space dimension of 2^4 . Specifically, $\{|\psi_k\rangle\}$ is chosen to be the eigenstates of coarse-grained H_∂ at the “infrared” end of MERA [28, 29, 40–42], with $k = 0, \dots, 15$ corresponding to increasing eigenvalues.

The hologrons, recently studied in the context of holographic models involving MERA [30, 34] are excited states created by flipping bulk spins of the ground state. A generic n -hologron state is defined as $|\Psi_n^{j_1, \dots, j_n}\rangle_h \equiv (\prod_{i=1}^n X_{j_i}) |\Psi_{\text{GS}}\rangle$, where X_j, Y_j, Z_j are Pauli operators acting on the j th bulk spin [30, 34]. Notably, intriguing static properties of these hologrons, such as the existence of an attractive potential between two hologrons that matches the prediction from AdS gravity, have been observed [34]. However, the question of their dynamical stability in the holographic model with H_∂ as the boundary remains unresolved.

To address this question, we numerically study the time evolution of the bulk system starting from a 1-hologron state and monitor the total probability of the bulk state $|\Psi(t)\rangle$ remaining within the 1-hologron subspace $\{|\Psi_{n=1}^j\rangle_h \mid j = 1, \dots, L-4\}$, i.e.,

$$P_1^h(t) \equiv \sum_{j=1}^{L-4} |\langle \Psi(t) | \Psi_{n=1}^j \rangle_h|^2. \quad (2)$$

Fig. 1(b) shows the dynamics of $P_1^h(t)$ for two initial states, $|\Psi_{n=1}^{j=7}\rangle_h$ and $|\Psi_{n=1}^{j=4}\rangle_h$, in a bulk system corresponding to $L = 16$ sites on the boundary. We observe that, in both cases, $P_1^h(t)$ rapidly decays from unity during time evolution. By fitting an exponential decay function, $Ae^{-t/\tau}$, to the numerical data in the time interval $[0, 1]$, we extract lifetimes for the single hologron: $\tau = 0.51$ for $|\Psi_{n=1}^{j=7}\rangle_h$ and $\tau = 0.85$ for $|\Psi_{n=1}^{j=4}\rangle_h$. These findings confirm that hologrons are not stable excitations in the bulk system with H_∂ as its holographic boundary. Further detailed checks on the stability of hologrons (see [42]) also confirm this conclusion.

Stable massive quasiparticles construction via boundary CFT primary operators.—Interestingly, Chua et al. [30] investigated a holographic model based on the MERA tensor network with a critical Ising chain as the holographic boundary, described by the Hamiltonian $H_{\text{C-Ising}} \equiv -L/(4\pi) \sum_{j=1}^L (Z_j + X_j X_{j+1})$, and demonstrated that the single hologron excitation is stable in this setup. A closer examination of the hologron excitation in

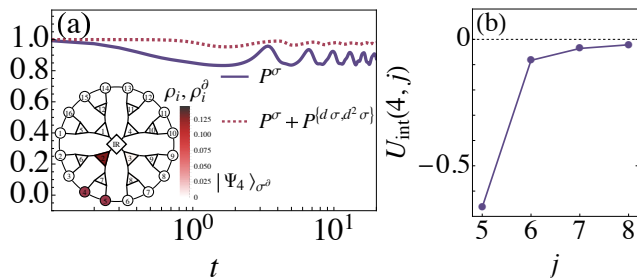


Figure 2. Dynamics and interactions of stable quasiparticles. (a) Time evolution of subspace probabilities for the initial boundary state $|\Psi_4\rangle_{\sigma^\partial}$. The inset shows the excitation densities ρ_i and ρ_i^∂ for $|\Psi_4\rangle_{\sigma^\partial}$. The color bar represents the value of ρ_i in the bulk and ρ_i^∂ on the boundary. (b) Interaction energies between quasiparticles $|\Psi_4\rangle_{\sigma^\partial}$ and $|\Psi_j\rangle_{\sigma^\partial}$ for $j = 5, 6, 7, 8$.

the holographic model from [30] reveals that the single-hologron subspace in the bulk is holographically mapped to the subspace on the boundary generated by single spin-flip operators X_j acting on the ground state. These operators serve as the leading-order lattice approximation of the primary operators in Ising CFT [43]. Through the operator-state correspondence in CFT [6], it follows that states generated by these spin-flip operators on the boundary are eigenstates and, thus, stable.

In contrast, for the holographic model considered here, the boundary system and the MERA tensor network differ from those in [30]. Consequently, the stability of the single-hologron subspace is not guaranteed, as its instability becomes evident during dynamical evolution [see Fig. 1(b)]. However, the above discussion suggests that the search for stable excitations in the bulk can be greatly facilitated by leveraging the local primary operators of the boundary system, a construction we will carry out in the following.

Although the boundary system H_∂ differs from $H_{C\text{-Ising}}$, both systems are described by the same Ising CFT in the low-energy limit [44, 45]. This suggests that we can construct stable boundary excitations using the primary operators of the Ising CFT. Specifically, we focus on the spin primary operator σ^{CFT} , which has the smallest non-trivial scaling dimension [6]. Its lattice realization, σ^∂ , for H_∂ can in principle be constructed using the variational method in [43]. Nevertheless, we directly utilize the unitary map $V \equiv \prod_j (iX_j X_{j+1} - I_j I_{j+1}) / \sqrt{2}$ that relates H_∂ and $H_{C\text{-Ising}}$ ($H_\partial = V^\dagger H_{C\text{-Ising}} V$) [41], together with the lattice realization of σ^{CFT} for $H_{C\text{-Ising}}$ [43], and are able to obtain

$$\sigma_j^\partial = V^\dagger [0.635(X_j + X_{j+1}) - 0.026(X_j Z_{j+1} + Z_j X_{j+1})] V, \quad (3)$$

where the subscript j specifies the lattice site. The corresponding single bulk excitation is then given by $|\Psi_j\rangle_{\sigma^\partial} = \mathcal{U}^\dagger \sigma_j^\partial \mathcal{U} |\Psi_{\text{GS}}\rangle$. To visualize this type of quasiparticles, we compute the bulk ‘‘excitation densities’’ $\rho_i \equiv \langle \Psi | (I +$

$Z_i) / 2 | \Psi \rangle - \langle \Psi_{\text{GS}} | (I + Z_i) / 2 | \Psi_{\text{GS}} \rangle$ and its boundary counterpart $\rho_i^\partial \equiv \langle \Phi^\partial | (I + Z_i) / 2 | \Phi^\partial \rangle - \langle \Phi_{\text{GS}}^\partial | (I + Z_i) / 2 | \Phi_{\text{GS}}^\partial \rangle$ with $|\Phi_{\text{GS}}^\partial\rangle = \mathcal{U} |\Psi_{\text{GS}}\rangle$ and $|\Phi^\partial\rangle = \mathcal{U} |\Psi\rangle$. As shown in the inset of Fig. 2(a), the excitation density for $|\Psi_4\rangle_{\sigma^\partial}$ is concentrated on a few bulk sites, indicating these quasiparticles are localized excitations in the AdS bulk.

From the inset of Fig. 2(a), it is evident that the quasiparticles constructed here receive notable contributions from single-site flipped bulk states, or hologrons. Thus, the mass of the hologrons, as identified in [34], is expected to confer mass to the quasiparticles constructed here. Since massive particles in AdS geometry are known to attract one another, it is reasonable to expect similar behavior for these quasiparticles. To validate this, we directly calculate the interaction energy $U_{\text{int}}(j, j')$ between two bulk quasiparticles generated by two boundary spin primary operators σ_j^∂ and $\sigma_{j'}^\partial$, i.e., $U_{\text{int}}(j, j') = \sigma^\partial \langle \Psi_{j, j'} | H | \Psi_{j, j'} \rangle_{\sigma^\partial} - \sigma^\partial \langle \Psi_j | H | \Psi_j \rangle_{\sigma^\partial} - \sigma^\partial \langle \Psi_{j'} | H | \Psi_{j'} \rangle_{\sigma^\partial}$, with $|\Psi_{j, j'}\rangle_{\sigma^\partial} \equiv \mathcal{U}^\dagger \sigma_j^\partial \sigma_{j'}^\partial \mathcal{U} |\Psi_{\text{GS}}\rangle$ representing the two-quasiparticle state. As shown in Fig. 2(b), all interaction energies are negative, indicating that these quasiparticles exhibit attractive interactions, consistent with the behavior of massive particles in AdS geometry.

While quasiparticles constructed from the primary operators of Ising CFT are stable in the thermodynamic limit, finite-size effects in experimentally realizable holographic models [34] can influence their stability. To examine this, we numerically simulate the real-time dynamics of the bulk system initialized in a single quasiparticle state $|\Psi_4\rangle_{\sigma^\partial}$, i.e., $|\Psi(t)\rangle = e^{-iHt} |\Psi_4\rangle_{\sigma^\partial}$, and monitor the probability $P^\sigma(t)$, which is the total probability of the bulk state remaining within the subspace spanned by all single-quasiparticle states $|\Psi_j\rangle_{\sigma^\partial}$, i.e., $\text{span}(\{|\Psi_j\rangle_{\sigma^\partial} | j = 1, 2, \dots, L\})$. As shown in Fig. 2(a), the late-time probability within this subspace is significantly enhanced compared to the case of the hologrons [see Fig. 1(b) for comparison] However, a decay of approximately 12% of $P^\sigma(t)$ is observed, which we attribute to the finite-size effects that cause the boundary system H^∂ to deviate from the low-energy Ising CFT description. To further analyze these deviations, we include the bulk subspace holographically mapped to the boundary subspace generated by the first and second derivative descendants, $(\partial_x \sigma^{\text{CFT}}, \partial_\tau \sigma^{\text{CFT}})$ and $(\partial_x^2 \sigma^{\text{CFT}}, \partial_\tau^2 \sigma^{\text{CFT}}, \partial_\tau \partial_x \sigma^{\text{CFT}})$, of the primary σ^{CFT} [6, 43], and calculate the total probability within this subspace $P^{(d\sigma, d^2\sigma)}$ (see [42] for the explicit forms of the lattice realization of the descendant operators and $P^{(d\sigma, d^2\sigma)}$). As shown in Fig. 2(a), the probability $P^\sigma + P^{(d\sigma, d^2\sigma)}$ reaches approximately 97.5% at late times. This suggests that couplings between subspaces generated by spin primary operators and their descendants, absent in the Ising CFT Hamiltonian, emerge in the finite-size boundary system H^∂ , largely accounting for the observed decay of $|\Psi_4\rangle_{\sigma^\partial}$.

Holographic transportation of boundary excitations via

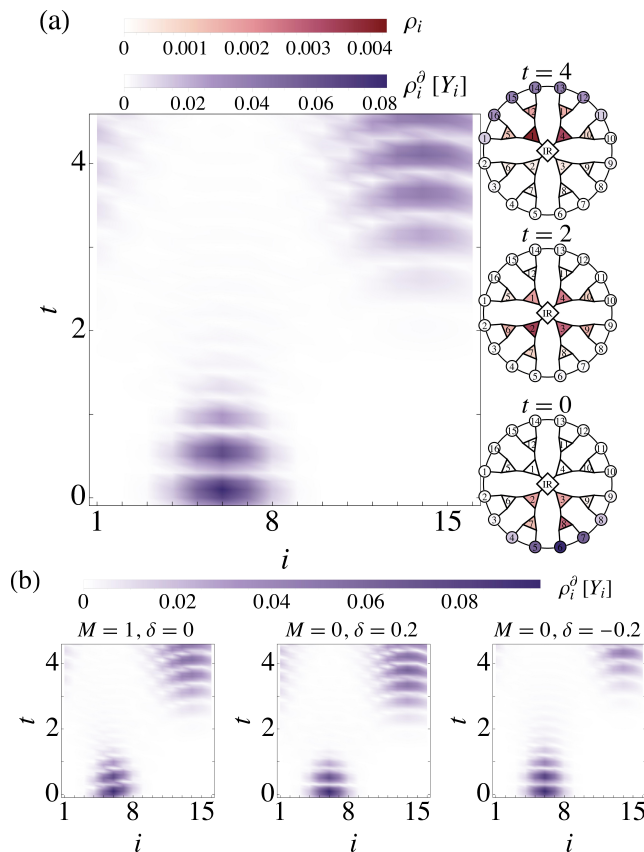


Figure 3. Holographic transportation of boundary excitations. (a) Dynamics of the ground state perturbed by Eq. (4) at $M=0$. The inset shows excitation densities ρ_i and $\rho_i^\theta [Y_i]$ at times $t=0, 2, 4$. The color bar indicates the value of ρ_i in the bulk and $\rho_i^\theta [Y_i]$ on the boundary. (b) Dynamics of the ground state perturbed by Eq. (4) under a Hamiltonian detuned from the critical point by an additional Δ -controlled term for $(M, \Delta) = (1, 0), (0, 0.2), (0, -0.2)$. All other parameters in (a, b) are set to $\Omega = 5, \sigma_t = \sigma_\phi = 0.4$. See text for more details.

AdS geodesics.—The above discussion demonstrated how the holographic map between the bulk and boundary facilitates the construction of stable quasiparticles in the bulk using the primary operators of boundary CFT. Here, we turn our attention to another aspect of this map: how the supposed AdS geometry of the bulk influences distinctive boundary physics.

Among many characteristic properties of the space-time geometry, geodesics hold a fundamental role. Recent studies on wave packets in the context of AdS/CFT correspondence [46, 47] suggest that perturbations in the boundary CFT can generate wave packets traveling along null geodesics in the AdS bulk. Specifically, the boundary value of the wave amplitude in the bulk is determined, to leading order, by the sum of the perturbation strength and the corresponding response strength (excitations on the boundary) [2, 3, 33, 46, 47]. This relationship implies that boundary excitations vanish as

the wave propagates through the AdS bulk but reappear when the wave reaches the boundary again. In other words, the boundary excitations undergo a process akin to being “transported” through the extra dimension of the holographic AdS bulk, a phenomenon we term “holographic transportation.” Notably, the recently discovered “spacetime-localized response” [48], derived via linear response theory in the critical Ising model, corresponds to this form of holographic transportation.

Since the holographic map \mathcal{U} between the bulk and boundary is explicitly constructed in the holographic model studied here, we can directly observe the “hidden” dynamics in the bulk during the holographic transportation of boundary excitations. Fig. 3 illustrates typical holographic transportation dynamics for boundary excitations under different system parameters. Specifically, boundary excitations are generated by perturbing the ground state $|\Phi_\theta^{\text{GS}}\rangle$ of the boundary system using a space-time localized source $\mathcal{J}_i(t)$ that couples to Y_i on the boundary, i.e., the perturbation on the boundary $\delta H_\theta(t)$ assumes the form

$$\delta H_\theta(t) = - \sum_{i=1}^L \mathcal{J}_i(t) Y_i, \quad (4)$$

where $\mathcal{J}_i(t) = A \exp \left[-(t^2/2\sigma_t^2) - (\phi_i^2/2\sigma_\phi^2) - i\Omega t + iM\phi_i \right]$ with $\phi_i = 2\pi i/L - 3\pi/4$. Here, Ω and M correspond to the energy and angular momentum of the geodesics in the bulk, respectively. The perturbation amplitude A is chosen as $A = \sqrt{2L/(\sigma_t\sigma_\phi)}/(40\pi)$, and σ_t and σ_ϕ control the temporal and spatial widths of the perturbation. To track the boundary dynamics, we define the excitation density for Y_i as $\rho_i^\theta [Y_i](t) \equiv \langle \Phi^\theta(t) | Y_i | \Phi^\theta(t) \rangle - \langle \Phi_{\text{GS}}^\theta | Y_i | \Phi_{\text{GS}}^\theta \rangle$.

As shown in Fig. 3(a), for the perturbation $\delta H_\theta(t)$ with parameters $(\Omega, \sigma_t, \sigma_\phi, M) = (5, 0.4, 0.4, 0)$, the boundary excitation emerges at $t \sim 0$, quickly vanishes at $t \sim 1.5$, and reappears at $t \sim 2.5$ (see the excitation density distribution $\rho_i^\theta [Y_i]$). Interestingly, during the interval when the boundary excitation vanishes, the excitation in the bulk propagates radially inward away from the boundary [middle inset of Fig. 3(a)]. And when this bulk excitation reaches the opposite side of the boundary [top inset of Fig. 3(a)], the boundary excitation re-emerges. This directly demonstrates that the boundary excitation undergoes holographic transportation through the extra dimension of the dual AdS bulk.

Experimental observability.—State-of-the-art quantum simulation platforms, such as trapped ions, superconducting qubits, and programmable Rydberg atom arrays [8, 9, 35–39, 49, 50], have made it feasible to implement MERA tensor networks for simulating holographic models in experimental settings. Specifically, using established experimental protocols [34] designed for Rydberg atom arrays, boundary states corresponding to the stable bulk quasiparticles constructed in this work—via

the boundary CFT primary operators—can be generated. The dynamics of these quasiparticles can also be observed experimentally through time evolution under the boundary Hamiltonian, followed by bulk-state reconstruction using a reverse MERA operation implemented with two-qubit gates [34].

Moreover, holographic transportation can be studied experimentally by introducing spacetime localized perturbations to the boundary system [see Eq. (4)], for instance, using focused laser pulses. The resulting dynamics can be observed by monitoring the excitation density distribution through fluorescence signals. Notably, holographic transportation exhibits robustness against possible experimental imperfections. As shown in Fig. 3(b), this phenomenon persists even under two types of deviations: (i) perturbations that introduce nonzero angular momentum M , or (ii) a boundary Hamiltonian slightly detuned from the critical point, assuming the form $H_\partial - \Delta \frac{L}{4\pi} \sum_{j=1}^L X_j X_{j+1}$ with $\Delta \neq 0$. In both cases, holographic transportation remains clearly observable, demonstrating its resilience under realistic experimental conditions.

Conclusions.—We have demonstrated that within the MERA model for AdS/CFT proposed in [34], while hologrons constructed via flipping bulk spins are dynamically unstable, stable bulk quasiparticles with attractive interactions can be constructed using the primary operators of the boundary Ising CFT. These quasiparticles offer a promising avenue for investigating open questions related to gravitational dynamics in the bulk. Additionally, we have identified a class of boundary excitations in this MERA model that exhibit holographic transportation—a phenomenon rooted in the AdS/CFT correspondence—where boundary excitations are transported through the bulk’s extra dimension. We believe our findings will inspire both further theoretical exploration of bulk dynamics in holographic models with gravitational analogs, particularly those associated with potential black holes, as well as experimental efforts to realize such holographic models and direct observation of typical dynamics characteristic of AdS/CFT correspondence, such as holographic transportation.

This work was supported by the National Key Research and Development Program of China (Grant No. 2022YFA1405300), the National Natural Science Foundation of China (Grant Nos. 12074180 and 12275089), Guangdong Basic and Applied Research Foundation (Grant Nos. 2023A1515012800), the Innovation Program for Quantum Science and Technology (Grant No. 2021ZD0301700).

* liang.he@scnu.edu.cn

[1] J. Maldacena, *International Journal of Theoretical*

- Physics* **38**, 1113 (1999).
- [2] S. Gubser, I. Klebanov, and A. Polyakov, *Physics Letters B* **428**, 105 (1998).
- [3] E. Witten, *Advances in Theoretical and Mathematical Physics* **2**, 253 (1998).
- [4] G. ’t Hooft, “Dimensional reduction in quantum gravity,” (2009), [arXiv:gr-qc/9310026](https://arxiv.org/abs/gr-qc/9310026).
- [5] L. Susskind, *Journal of Mathematical Physics* **36**, 6377 (1995).
- [6] P. Francesco, P. Mathieu, and D. Sénéchal, *Conformal field theory* (Springer Science & Business Media, 2012).
- [7] C. Monroe, W. C. Campbell, L.-M. Duan, Z.-X. Gong, A. V. Gorshkov, P. W. Hess, R. Islam, K. Kim, N. M. Linke, G. Pagano, P. Richerme, C. Senko, and N. Y. Yao, *Rev. Mod. Phys.* **93**, 025001 (2021).
- [8] R. Haghshenas, E. Chertkov, M. DeCross, T. M. Gatterman, J. A. Gerber, K. Gilmore, D. Gresh, N. Hewitt, C. V. Horst, M. Matheny, T. Mengle, B. Neyenhuis, D. Hayes, and M. Foss-Feig, *Phys. Rev. Lett.* **133**, 266502 (2024).
- [9] A. Keesling, A. Omran, H. Levine, H. Bernien, H. Pichler, S. Choi, R. Samajdar, S. Schwartz, P. Silvi, S. Sachdev, P. Zoller, M. Endres, M. Greiner, V. Vuletić, and M. D. Lukin, *Nature* **568**, 207 (2019).
- [10] K. Slagle, D. Aasen, H. Pichler, R. S. K. Mong, P. Fendley, X. Chen, M. Endres, and J. Alicea, *Phys. Rev. B* **104**, 235109 (2021).
- [11] F. Fang, K. Wang, V. S. Liu, Y. Wang, R. Cimmino, J. Wei, M. Bintz, A. Parr, J. Kemp, K.-K. Ni, and N. Y. Yao, “Probing critical phenomena in open quantum systems using atom arrays,” (2024), [arXiv:2402.15376](https://arxiv.org/abs/2402.15376).
- [12] S. Kim, A. Lukin, M. Rispoli, M. E. Tai, A. M. Kaufman, P. Segura, Y. Li, J. Kwan, J. Léonard, B. Bakkali-Hassani, and M. Greiner, “Adiabatic state preparation in a quantum ising spin chain,” (2024), [arXiv:2404.07481](https://arxiv.org/abs/2404.07481).
- [13] S. Sachdev and J. Ye, *Phys. Rev. Lett.* **70**, 3339 (1993).
- [14] A. Kitaev, “A simple model of quantum holography,” Talks at KITP, April 7, 2015 and May 27, 2015 (2015), [kavli Institute for Theoretical Physics \(KITP\)](https://www.kitp.ucsb.edu).
- [15] J. Maldacena and D. Stanford, *Phys. Rev. D* **94**, 106002 (2016).
- [16] S. Xu, L. Susskind, Y. Su, and B. Swingle, “A sparse model of quantum holography,” (2020), [arXiv:2008.02303](https://arxiv.org/abs/2008.02303).
- [17] D. Jafferis, A. Zlokapa, J. D. Lykken, D. K. Kolchmeyer, S. I. Davis, N. Lauk, H. Neven, and M. Spiropulu, *Nature* **612**, 51 (2022).
- [18] T. Banks, W. Fischler, S. H. Shenker, and L. Susskind, *Phys. Rev. D* **55**, 5112 (1997).
- [19] N. Itzhaki, J. M. Maldacena, J. Sonnenschein, and S. Yankielowicz, *Phys. Rev. D* **58**, 046004 (1998).
- [20] M. Hanada, Y. Hyakutake, G. Ishiki, and J. Nishimura, *Science* **344**, 882 (2014).
- [21] E. Berkowitz, E. Rinaldi, M. Hanada, G. Ishiki, S. Shimasaki, and P. Vranas (Monte Carlo String/M-Theory Collaboration (MCSMC)), *Phys. Rev. D* **94**, 094501 (2016).
- [22] E. Rinaldi, X. Han, M. Hassan, Y. Feng, F. Nori, M. McGuigan, and M. Hanada, *PRX Quantum* **3**, 010324 (2022).
- [23] S. Pateloudis, G. Bergner, M. Hanada, E. Rinaldi, A. Schäfer, P. Vranas, H. Watanabe, N. Bodendorfer, and T. M. C. S. theory (MCSMC) collaboration, *Journal of High Energy Physics* **2023**, 71 (2023).

- [24] J. Maldacena, “A simple quantum system that describes a black hole,” (2023), [arXiv:2303.11534](#).
- [25] B. Kobrin, Z. Yang, G. D. Kahanamoku-Meyer, C. T. Olund, J. E. Moore, D. Stanford, and N. Y. Yao, *Phys. Rev. Lett.* **126**, 030602 (2021).
- [26] A. M. García-García, C. Liu, and J. J. M. Verbaarschot, “Sparsity independent lyapunov exponent in the sachdev-ye-kitaev model,” (2023), [arXiv:2311.00639 \[hep-th\]](#).
- [27] B. Swingle, *Phys. Rev. D* **86**, 065007 (2012).
- [28] G. Vidal, *Phys. Rev. Lett.* **101**, 110501 (2008).
- [29] G. Vidal, *Phys. Rev. Lett.* **99**, 220405 (2007).
- [30] V. Chua, V. Passias, A. Tiwari, and S. Ryu, *Phys. Rev. B* **95**, 195152 (2017).
- [31] X.-L. Qi, “Exact holographic mapping and emergent space-time geometry,” (2013), [arXiv:1309.6282](#).
- [32] D. Harlow, “Tasi lectures on the emergence of the bulk in ads/cft,” (2018), [arXiv:1802.01040](#).
- [33] T. Banks, M. R. Douglas, G. T. Horowitz, and E. Martinec, “Ads dynamics from conformal field theory,” (1998), [arXiv:hep-th/9808016](#).
- [34] R. Sahay, M. D. Lukin, and J. Cotler, “Emergent holographic forces from tensor networks and criticality,” (2024), [arXiv:2401.13595](#).
- [35] H. Bernien, S. Schwartz, A. Keesling, H. Levine, A. Omran, H. Pichler, S. Choi, A. S. Zibrov, M. Endres, M. Greiner, V. Vuletić, and M. D. Lukin, *Nature* **551**, 579 (2017).
- [36] S. Ebadi, T. T. Wang, H. Levine, A. Keesling, G. Semeghini, A. Omran, D. Bluvstein, R. Samajdar, H. Pichler, W. W. Ho, S. Choi, S. Sachdev, M. Greiner, V. Vuletić, and M. D. Lukin, *Nature* **595**, 227 (2021).
- [37] P. Scholl, M. Schuler, H. J. Williams, A. A. Eberharter, D. Barredo, K.-N. Schymik, V. Lienhard, L.-P. Henry, T. C. Lang, T. Lahaye, A. M. Läuchli, and A. Browaeys, *Nature* **595**, 233 (2021).
- [38] G. Semeghini, H. Levine, A. Keesling, S. Ebadi, T. T. Wang, D. Bluvstein, R. Verresen, H. Pichler, M. Kalinowski, R. Samajdar, A. Omran, S. Sachdev, A. Vishwanath, M. Greiner, V. Vuletić, and M. D. Lukin, *Science* **374**, 1242 (2021).
- [39] D. Bluvstein, H. Levine, G. Semeghini, T. T. Wang, S. Ebadi, M. Kalinowski, A. Keesling, N. Maskara, H. Pichler, M. Greiner, V. Vuletić, and M. D. Lukin, *Nature* **604**, 451 (2022).
- [40] G. Evenbly and G. Vidal, *Phys. Rev. B* **79**, 144108 (2009).
- [41] G. Evenbly and S. R. White, *Phys. Rev. Lett.* **116**, 140403 (2016).
- [42] See the Supplementary Material for a discussion on relevant technical details.
- [43] Y. Zou, A. Milsted, and G. Vidal, *Phys. Rev. Lett.* **124**, 040604 (2020).
- [44] R. Verresen, R. Thorngren, N. G. Jones, and F. Pollmann, *Phys. Rev. X* **11**, 041059 (2021).
- [45] N. G. Jones and R. Verresen, *J. Stat. Phys.* **175**, 1164 (2019).
- [46] S. Terashima, *Phys. Rev. D* **109**, 106012 (2024).
- [47] S. Kinoshita, K. Murata, and D. Takeda, *Journal of High Energy Physics* **2023**, 74 (2023).
- [48] M. Bamba, K. Hashimoto, K. Murata, D. Takeda, and D. Yamamoto, *Phys. Rev. D* **109**, 126003 (2024).
- [49] S. A. Moses, C. H. Baldwin, M. S. Allman, R. Ancona, L. Ascarrunz, C. Barnes, J. Bartolotta, B. Bjork, P. Blanchard, M. Bohn, J. G. Bohnet, N. C. Brown, N. Q. Burdick, W. C. Burton, S. L. Campbell, J. P. Campora, C. Carron, J. Chambers, J. W. Chan, Y. H. Chen, A. Chernoguzov, E. Chertkov, J. Colina, J. P. Curtis, R. Daniel, M. DeCross, D. Deen, C. Delaney, J. M. Dreiling, C. T. Ertsgaard, J. Esposito, B. Estey, M. Fabrikant, C. Figgatt, C. Foltz, M. Foss-Feig, D. Francois, J. P. Gaebler, T. M. Gatterman, C. N. Gilbreth, J. Giles, E. Glynn, A. Hall, A. M. Hankin, A. Hansen, D. Hayes, B. Higashi, I. M. Hoffman, B. Horning, J. J. Hout, R. Jacobs, J. Johansen, L. Jones, J. Karcz, T. Klein, P. Lauria, P. Lee, D. Liefer, S. T. Lu, D. Lucchetti, C. Lytle, A. Malm, M. Matheny, B. Mathewson, K. Mayer, D. B. Miller, M. Mills, B. Neyenhuis, L. Nugent, S. Olson, J. Parks, G. N. Price, Z. Price, M. Pugh, A. Ransford, A. P. Reed, C. Roman, M. Rowe, C. Ryan-Anderson, S. Sanders, J. Sedlacek, P. Shevchuk, P. Siegfried, T. Skripka, B. Spaun, R. T. Sprenkle, R. P. Stutz, M. Swallows, R. I. Tobey, A. Tran, T. Tran, E. Vogt, C. Volin, J. Walker, A. M. Zolot, and J. M. Pino, *Phys. Rev. X* **13**, 041052 (2023).
- [50] F. Arute, K. Arya, R. Babbush, D. Bacon, J. C. Bardin, R. Barends, R. Biswas, S. Boixo, F. G. S. L. Brandao, D. A. Buell, B. Burkett, Y. Chen, Z. Chen, B. Chiaro, R. Collins, W. Courtney, A. Dunsworth, E. Farhi, B. Foxen, A. Fowler, C. Gidney, M. Giustina, R. Graff, K. Guerin, S. Habegger, M. P. Harrigan, M. J. Hartmann, A. Ho, M. Hoffmann, T. Huang, T. S. Humble, S. V. Isakov, E. Jeffrey, Z. Jiang, D. Kafri, K. Kechedzhi, J. Kelly, P. V. Klimov, S. Knysh, A. Korotkov, F. Kostritsa, D. Landhuis, M. Lindmark, E. Lucero, D. Lyakh, S. Mandrà, J. R. McClean, M. McEwen, A. Megrant, X. Mi, K. Michielsen, M. Mohseni, J. Mutus, O. Naaman, M. Neeley, C. Neill, M. Y. Niu, E. Ostby, A. Petukhov, J. C. Platt, C. Quintana, E. G. Rieffel, P. Roushan, N. C. Rubin, D. Sank, K. J. Satzinger, V. Smelyanskiy, K. J. Sung, M. D. Trevithick, A. Vainsencher, B. Villalonga, T. White, Z. J. Yao, P. Yeh, A. Zalcman, H. Neven, and J. M. Martinis, *Nature* **574**, 505 (2019).

Supplemental Material for “Stable excitations and holographic transportation in tensor networks of critical spin chains”

I. DETAILS FOR NUMERICAL IMPLEMENTATION

To be self-contained, we outline the minimal procedures for implementing the MERA toy model proposed in Ref. [34], and provide additional details of our numerical implementation.

We first note that the Hamiltonians and ground states in both the bulk and the boundary are represented as follows:

$$\begin{array}{ccc} \text{bulk} & \longleftrightarrow & \text{boundary} \\ H & & H_\partial = \mathcal{U}H\mathcal{U}^\dagger \\ |\Psi_{\text{GS}}\rangle & & |\Psi_{\text{GS}}^\partial\rangle = \mathcal{U}|\Psi_{\text{GS}}\rangle. \end{array} \quad (\text{S1})$$

The unitary mapping \mathcal{U} is determined by

$$\mathcal{U} = \prod_{\ell=2}^{D-1} \left(\prod_{j=1}^{2^\ell} u_{2j,2j+1} \right) w^{\otimes 2^\ell}, \quad (D \equiv \log_2 L) \quad (\text{S2})$$

where the analytic expressions for u^\dagger and w^\dagger are given by [41]

$$\begin{aligned} u_{j,j+1}^\dagger &= \frac{\sqrt{3}+2}{4} I_j I_{j+1} + \frac{\sqrt{3}-2}{4} Z_j Z_{j+1} \\ &\quad + \frac{i}{4} X_j Y_{j+1} + \frac{i}{4} Y_j X_{j+1}, \end{aligned} \quad (\text{S3})$$

$$\begin{aligned} w_{j,j+1}^\dagger &= \frac{\sqrt{3}+\sqrt{2}}{4} I_j I_{j+1} + \frac{\sqrt{3}-\sqrt{2}}{4} Z_j Z_{j+1} \\ &\quad + i \frac{1+\sqrt{2}}{4} X_j Y_{j+1} + i \frac{1-\sqrt{2}}{4} Y_j X_{j+1}. \end{aligned} \quad (\text{S4})$$

Both u and w are represented by 4-leg tensors in the MERA network.

At the operator level, given a boundary Hamiltonian H_∂ and the mapping \mathcal{U} , the bulk Hamiltonian is implicitly known. Since we can equivalently simulate the bulk dynamics via the boundary system, we do not need an explicit formula for H .

At the state level, given the boundary ground state, the bulk ground state $|\Psi_{\text{GS}}\rangle$ can be determined. Since we are interested in the excitations above $|\Psi_{\text{GS}}\rangle$, we must first determine the bulk spin configuration of $|\Psi_{\text{GS}}\rangle$. The ground state is constructed as

$$|\Psi_{\text{GS}}\rangle = |0\rangle^{\otimes(L-4)} \otimes |\psi_0\rangle, \quad (\text{S5})$$

where the $L-4$ bulk spins are polarized in the state $|0\rangle$ satisfying $\mathcal{Z}|0\rangle = |0\rangle$, and the remaining 4 bulk spins in the infrared region are described by $|\psi_0\rangle$. The infrared state $|\psi_0\rangle$ is unknown and must be determined in order to minimize the ground state energy,

$$E_{\text{GS}} = \langle \Psi_{\text{GS}} | \mathcal{U}^\dagger H_\partial \mathcal{U} | \Psi_{\text{GS}} \rangle. \quad (\text{S6})$$

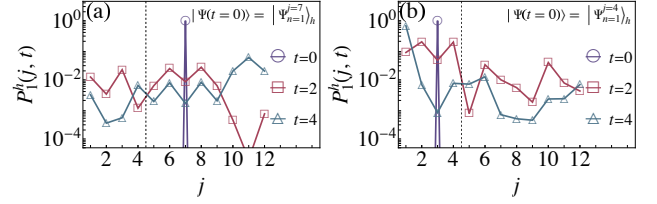


Figure S1. Dynamics of hologrons. (a, b) Time evolution of site-resolved probabilities $P_1^h(j, t)$ for initial bulk states $|\Psi_{n=1}^{j=7}\rangle_h$ and $|\Psi_{n=1}^{j=4}\rangle_h$. See text for more details.

To achieve this, we need to express E_{GS} in terms of $|\psi_0\rangle$. Due to the renormalization process of the MERA network, $|\psi_0\rangle$ is the infrared state of $|\Psi_{\text{GS}}^\partial\rangle$ after coarse-graining. The energy can be equivalently expressed as

$$\begin{aligned} E_{\text{GS}} &= \langle \psi_0 | \mathcal{A}^{D-2} [H_\partial] | \psi_0 \rangle \\ &= \frac{L}{4\pi} \sum_{j=1}^L \langle \psi_0 | \mathcal{A}^{D-2} [X_{j-1} Z_j X_{j+1} - X_j X_{j+1}] | \psi_0 \rangle, \end{aligned} \quad (\text{S7})$$

where \mathcal{A} is the so-called ascending superoperator, and \mathcal{A}^{D-2} performs coarse-graining for $D-2$ iterations. In practice, the action of \mathcal{A} on an operator is computed via tensor contractions, as illustrated in [34]. After obtaining $\mathcal{A}^{D-2} [H_\partial]$, which is a 16×16 matrix, we can simply diagonalize it, and $|\psi_0\rangle$ is taken as its ground state. The remaining 15 excited states are labeled by $\{|\psi_k\rangle\}$ with $k = 1, \dots, 15$.

In our numerical calculation, the exact ground state energy of the boundary spin chain is $\langle \Psi_{\text{GS}}^\partial | H_\partial | \Psi_{\text{GS}}^\partial \rangle \approx -25.9799$, while the ground state energy from the MERA ansatz is $\langle \Psi_{\text{GS}} | \mathcal{U}^\dagger H_\partial \mathcal{U} | \Psi_{\text{GS}} \rangle \approx -25.3972$, with a relative error of 2.24%. The overlap between the exact ground state and ansatz ground state is $|\langle \Psi_{\text{GS}}^\partial | \mathcal{U} | \Psi_{\text{GS}} \rangle| \approx 0.9525$.

II. MORE EVIDENCE FOR HOLOGRON'S INSTABILITY

Here, we provide further evidence supporting the instability of hologrons. To investigate the behavior of a single hologron during time evolution, we calculate the site-resolved probabilities

$$P_1^h(j, t) \equiv \left| \langle \Psi(t) | \Psi_{n=1}^j \rangle_h \right|^2, \quad (\text{S8})$$

where the total probability shown in Fig. 1(b) is given by $P_1^h(t) = \sum_{j=1}^{L-4} P_1^h(j, t)$. As illustrated in Fig. S1(a), a hologron initially located at $j=7$ propagates across

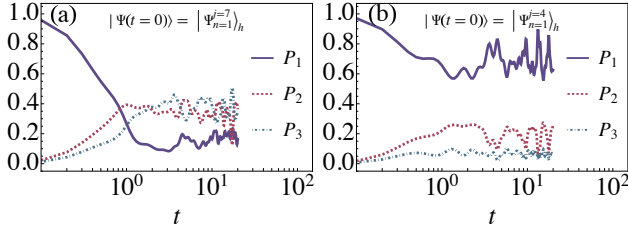


Figure S2. Instability of hologrons in the generalized hologron subspace. (a, b) Time evolution of subspace probabilities for initial states $|\Psi_{n=1}^{j=7}\rangle_h$ (a) and $|\Psi_{n=1}^{j=4}\rangle_h$ (b).

the MERA tensor network to the opposite side, reaching sites $j = 10, 11, 12$ with both positive and negative angular momentum during the time interval $t = 0$ to $t = 4$. Similarly, in Fig. S1(b), a hologron initially at $j = 4$ moves to $j = 1$, which is situated on the other side of the network, at $t = 4$. However, in both cases, the total probability rapidly decreases by nearly an order of magnitude at $t = 2$, consistent with the findings in Fig. 1(b).

We observe that the multi-hologron states, defined by flipping bulk spins in the ground state, cannot fully span the Hilbert space due to the residual 2^4 -dimensional degrees of freedom in the infrared region. This incomplete basis of hologron states may explain their instability. To explore this further, we introduce a generalized hologron state defined as

$$|\Psi_{n,k}^{j_1, \dots, j_n}\rangle_h \equiv \left(\prod_{i=1}^n \chi_{j_i} \right) |0\rangle^{\otimes(L-4)} \otimes |\psi_k\rangle, \quad (\text{S9})$$

where $k = 0, \dots, 15$ and $|\Psi_{n,k=0}^{j_1, \dots, j_n}\rangle_h$ reduces to the original ground-state-based hologron $|\Psi_n^{j_1, \dots, j_n}\rangle_h$. Using this generalization, we simulate the dynamics and track the total probability of the bulk state $|\Psi(t)\rangle$ remaining within the generalized n -hologron subspace, defined as $\{|\Psi_{n,k}^j\rangle_h \mid j = 1, \dots, L-4; k = 0, \dots, 15\}$, i.e.,

$$P_n(t) \equiv \sum_{k=0}^{15} \sum_{j=1}^{L-4} |\langle \Psi(t) | \Psi_{n,k}^j \rangle_h|^2. \quad (\text{S10})$$

Fig. S2 displays the dynamics of $P_n(t)$ for $n = 1, 2, 3$ starting from the initial bulk states $|\Psi_{n=1}^{j=7}\rangle_h$ and $|\Psi_{n=1}^{j=4}\rangle_h$. In Fig. S2(a), the single hologron $|\Psi_{n=1}^{j=7}\rangle_h$ still exhibits rapid decay within the generalized 1-hologron subspace, with a lifetime $\tau = 0.76$ (fitted with $Ae^{-t/\tau}$ for $0 < t < 1$). Meanwhile, probabilities for higher-dimensional subspaces, such as $P_2(t)$ and $P_3(t)$, quickly increase, indicating the decay of a single hologron into generalized hologron pairs and triples. Similarly, as shown in Fig. S2(b), the single hologron $|\Psi_{n=1}^{j=4}\rangle_h$ exhibits an enhanced lifetime of $\tau = 2.39$, but still decays, reaffirming its instability.

Since unitary time evolution conserves energy, we anticipate that the instability of hologrons will be evident

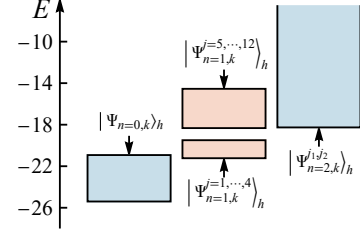


Figure S3. Energy ranges of hologrons and generalized hologrons. Depicted are the energy ranges for $|\Psi_{n=0,k}\rangle_h$, $|\Psi_{n=1,k}^{j_1, j_2}\rangle_h$, and $|\Psi_{n=2,k}^{j_1, j_2}\rangle_h$, with varying j and k .

in the energy spectrum. As shown in Fig. S3, we compute the energy expectation values for all possible (generalized) 0-, 1- and 2-hologron states. Indeed, from structures of the possible energy ranges of different generalized n -hologron states, one expects that the decay of a single hologron can easily happen, since there is no obvious large energy gap that separates the generalized 1-hologron subspace from other generalized multiple-hologron subspaces.

III. LATTICE REALIZATION OF DERIVATIVE DESCENDANTS

From the relations provided in Table I of [43], we observe the following approximate correspondences

$$Y_j \sim 0.8031i\partial_\tau \sigma^{\text{CFT}},$$

$$X_j \sim 0.803121\sigma^{\text{CFT}} - 0.017\partial_x^2 \sigma^{\text{CFT}} \quad (\text{S11})$$

$$-0.033\partial_x^2 \sigma^{\text{CFT}}, \quad (\text{S12})$$

$$X_j Z_{j+1} + Z_j X_{j+1} \sim 0.803121\sigma^{\text{CFT}} - 0.820\partial_\tau^2 \sigma^{\text{CFT}} - 0.736\partial_x^2 \sigma^{\text{CFT}}, \quad (\text{S13})$$

$$X_j Z_{j+1} - Z_j X_{j+1} \sim 1.205\partial_x \sigma^{\text{CFT}}, \quad (\text{S14})$$

$$Y_j Z_{j+1} + Z_j Y_{j+1} \sim 2.41i\partial_\tau \sigma^{\text{CFT}}, \quad (\text{S15})$$

$$Y_j Z_{j+1} - Z_j Y_{j+1} \sim -0.4015i\partial_\tau \partial_x \sigma^{\text{CFT}}. \quad (\text{S16})$$

These relations suggest that the subspace consisting of the spin primary states and their first and second derivative descendants is defined as

$$\mathcal{V} \equiv \text{span}(\{\mathcal{U}^\dagger A_j \mathcal{U} |\Psi_{\text{GS}}\rangle_{A_j, j}\}), \quad (\text{S17})$$

where A_j runs over the set $\{X_j, Y_j, X_j Z_{j+1}, Z_j X_{j+1}, Y_j Z_{j+1}, Z_j Y_{j+1}\}$ and j runs over $\{1, 2, \dots, L\}$. Thus, we define the subspace of first- and second-derivative descendants as

$$\mathcal{V}/\text{span}(\{|\Psi_j\rangle_{\sigma^\partial} | j\}). \quad (\text{S18})$$

The probability of a state within this subspace is $\mathcal{P}\{d\sigma, d^2\sigma\}$ in Fig. 2(a).